

# Morphology and Associated Surface Chemistry of L-Isoleucine Crystals Modeled under the Influence of L-Leucine Additive Molecules

Published as part of a virtual special issue of selected papers presented at the 9th International Workshop on the Crystal Growth of Organic Materials (CGOM9).

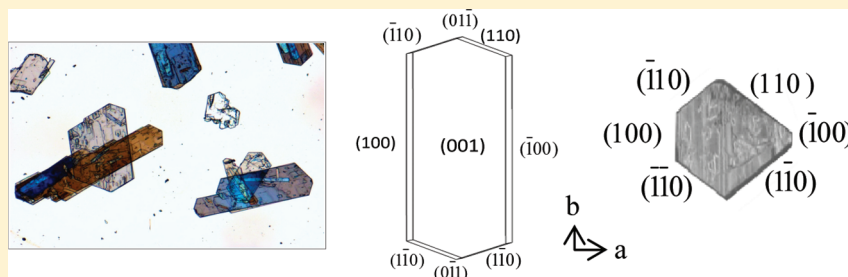
Nornizar Anuar,\*<sup>§</sup> Wan Ramli Wan Daud,<sup>‡</sup> Kevin J. Roberts,<sup>†</sup> Siti Kartom Kamarudin,<sup>‡</sup> and Siti Masrinda Tasirin<sup>‡</sup>

\*Faculty of Chemical Engineering, Universiti Teknologi MARA, 40450 Shah Alam, Selangor, Malaysia

†Department of Chemical and Process Engineering, Universiti Kebangsaan Malaysia, 43600, Bangi, Selangor, Malaysia

<sup>‡</sup>Institute of Particle Science and Engineering and Institute for Process R&D, School of Process, Environment and Material Engineering, University of Leeds, Leeds LS2 9JT, United Kingdom

## S Supporting Information



**ABSTRACT:** Molecular modeling techniques using both the empirical atom–atom and ab initio quantum mechanical methods are used to simulate the morphology of L-isoleucine. The lattice energy calculated by using a selected potential function and an atomic charge set is in excellent agreement with experimental data where the percentage difference between the calculated and experimental lattice energies is less than 5%, hence confirming the suitability of the potential functions and methods chosen to calculate the partial atomic charges. Calculation of the atom–atom interactions also shows that the energy contribution to the lattice energy is dominated by the interatomic interactions between the carbonyl oxygens and the amino hydrogens, consistent with the large calculated electrostatic contribution to the lattice energy. The simulated crystal morphology shows an elongated hexagonal platelike morphology with dominant crystal facets of (001) and (001̄) together with minor (100), (100̄), (110), (110̄), (110), (110̄), (011̄), and (011) faces. Experimental studies of the closely related amino acid L-leucine as an additive to L-isoleucine reveal that the addition of L-leucine alters L-isoleucine morphology, forming a more isometric hexagonal shape crystal by reducing the growth along the *b*-axis of the L-isoleucine crystal. This observation is supported by modeling through assessment of binding of L-leucine on preferential sites of the crystal habit surfaces of L-isoleucine where additive binding is found to be most preferred on the (100), (100̄), (110), and (011̄) facets.

## INTRODUCTION

Amino acids, the fundamental building blocks for the self-assembly of polypeptides and proteins, are materials with significant importance in many applications in the pharmaceutical, food, and fine chemical industries. Predicting amino acids morphology and understanding the phenomenon of the self-assembly and molecular interaction of solvent and additive molecules in the host crystal interface<sup>1–5</sup> have been topical and attractive areas for fundamental research. As an example, in the case of glycine with additive, the crystallographic change of its morphology is due to the electrostatic repulsive interactions between anionic and  $\alpha$ -glycine molecules at the enantiotropic faces and the interaction of molecular speciation of additives.<sup>6</sup>

The charged glycine species were found to selectively inhibit the nucleation and crystal growth of  $\alpha$ -glycine, resulting in the formation of  $\gamma$ -glycine.<sup>7</sup> Manipulation of the growth of this polymorph by racemic hexafluorovaline additive on glycine has also been carried out<sup>8</sup> on the basis of the knowledge of exposed surface chemistry and intermolecular arrangement, i.e. the centrosymmetric form in  $\alpha$ -glycine and the polar form in  $\gamma$ -glycine.

L-Isoleucine represents an attractive model compound due to both its interesting crystal chemistry and its varied surface

Received: June 14, 2011

Revised: January 31, 2012

Published: February 13, 2012



properties, while L-leucine has been selected as the additive to L-isoleucine. The later reflects its presence as a byproduct during L-isoleucine production via fermentation and due to their similar metabolic pathways, leading to the possibility of impurity incorporation into the L-isoleucine structure during crystallization.<sup>9</sup> Both these compounds have a nonpolar hydrophobic side-group and have low and similar solubility characteristics in water, thus making the separation process for these materials challenging. There have been some recent studies of L-isoleucine crystallization, for example, resolved molecular structure,<sup>10</sup> solubility and solution activity,<sup>11–14</sup> molecular conformation,<sup>15</sup> morphology prediction,<sup>16</sup> Raman spectra pattern,<sup>17</sup> and possible new polymorphic form of L-isoleucine.<sup>14</sup> The effect of impurities on L-isoleucine crystal morphology also has been reported.<sup>18–20</sup> The use of L-isoleucine as one of the test materials from the hydrophobic amino acids group in a molecular modeling work revealed new details in the interactions between the side chains, surrounding donors and acceptor molecules. The ab initio method used in this modeling work also showed the estimation of inductive effects of its side chain on the total interaction energy.<sup>21</sup> From the lattice energy calculation based on the structure minimization method, Day and Cooper<sup>15</sup> predicted that DL-isoleucine is capable of having a more stable structure than the known racemate crystal structure.

In this paper, the morphology prediction of L-isoleucine, the intermolecular and interatomic interactions within L-isoleucine, and the preferential L-leucine incorporation on L-isoleucine surfaces by using established computational techniques are presented.

**Theoretical Background on Computational Modeling.** The external morphology of a crystal can be predicted with reasonable success from its internal structure by calculating the intermolecular forces associated with the slice energy,  $E_{sl}$  (the energy released when a growth layer of thickness  $d_{hkl}$  is formed), and the attachment energy,  $E_{att}$  (the energy released on the addition of this slice to the  $hkl$  surface of a growing crystal), of crystallizing units.<sup>22</sup> The summation of these energies is the total lattice energy ( $E_{latt}$ ) of a crystal.

$$E_{latt} = E_{sl} + E_{att} \quad (1)$$

The crystal face with the lowest attachment energy is the slowest growing area and has the largest surface area and the most morphological important crystal faces.<sup>23</sup> The  $E_{sl}$  and  $E_{att}$  can be calculated by summing in pairs the potential energy involved in the intermolecular interactions between a central molecule and all the molecules within and outwith of slice thickness  $d_{hkl}$ .<sup>25</sup> The lattice energies of various organic acids determined using the summation of intermolecular interaction method have been successfully validated by Roberts and co-workers<sup>24–28</sup> by using eq 2;

$$E_{latt} = -\Delta H_{sub} - 2RT \quad (2)$$

where  $E_{latt}$  is the lattice energy,  $\Delta H_{sub}$  is the enthalpy of sublimation,  $R$  is the gas constant, and  $T$  is the temperature. However, the lattice energies of amino acids calculated using ab initio quantum mechanical methods are much higher (ca. 60 kcal/mol) than those calculated using the summation of intermolecular interactions. This discrepancy could be due to an underestimation of the electrostatic interactions between zwitterions molecules in a solid-state.<sup>29</sup> Most amino acids exist as zwitterions in crystal and liquid phases but change to neutral form in the gas phase upon sublimation through intramolecular

proton transfer from a  $\text{NH}_3^+$  group or a  $\text{COO}^-$  group.<sup>30,31</sup> The difference of molecular energy between the neutral form in the gas phase and the zwitterion form is known as the proton transfer energy,<sup>31</sup>  $\Delta E_{pt}$ . Thus, in this work, eq 2 was modified to include the proton transfer expression, which then becomes<sup>30</sup>

$$E_{latt} = -\Delta H_{sub} - 2RT + \Delta E_{pt} \quad (3)$$

It is also believed that the lattice energy calculated by using an isolated molecule could underestimate the total lattice energy of the crystal in which the molecular properties (energy and electron density distribution) of the packed structure due to the polarization effect of cluster molecules were not taken into account.<sup>32</sup> The polarization effect due to polarization of the molecular charge density by the crystal environment has been shown to be necessary for modeling the balance between inter- and intramolecular interactions. The polar environments in crystals of hydrogen bonded molecules also are known to strengthen electrostatic interactions between molecules, depending on the relative arrangement of the polar functional group.<sup>33</sup>

## MATERIALS AND METHODS

**Materials and Crystallization Method.** In this work, both L-isoleucine ( $\text{C}_6\text{H}_{13}\text{O}_2\text{N}$ , MW = 131.2, purity of 99.6%) and the additive L-leucine ( $\text{C}_6\text{H}_{13}\text{O}_2\text{N}$ , MW = 131.2, purity  $\geq 99\%$ ) were purchased from MERCK. Both pure L-isoleucine and L-isoleucine with L-leucine incorporation crystals shown in this work were recovered from the crystallization process. They were carried out in a batch cooling crystallizer with a cooling rate of 0.5 °C/min. The concentration of the host material was kept at 44 g/L, and L-leucine was added as the weight % of the host material. Distilled water was used to make up the solution.

**Crystal Structures.** The crystal structures of L-isoleucine and L-leucine were obtained from the Cambridge Structural Database (CSD) (ref code: LISLEU02 and LEUCINE02, respectively). L-Isoleucine crystallizes in a monoclinic lattice with space group  $P2_1$ ,  $Z = 4$ , and cell parameters  $a = 9.6810$ ,  $b = 5.3010$ ,  $c = 13.9560$  Å, and  $\beta = 96.160^\circ$ . L-Isoleucine is packed with four molecules with two bimolecular asymmetric units in the unit cell. Both independent molecules in the asymmetric unit (A and B) have the ability to rotate about their two chiral centers,  $C_\alpha$  and  $C_\beta$ , with *gauche I* and *trans* rotation, respectively, which results in different atomic R group positions in the unit cell, atomic bond lengths, and angle conformations.<sup>34</sup> L-Isoleucine molecules are packed alternately between molecules A and B in the crystal lattice structure (Figure 1a), and the conformational difference between both molecules results in different hydrogen bond patterns between the molecules and between the asymmetric pairs in the crystal packing.<sup>35</sup> L-Isoleucine molecules are packed within the unit cell in a manner that creates regions of hydrophilic and hydrophobic nature, with the hydrophilic regions involving the hydrogen bond network, while the hydrophobic regions are associated with van der Waals interactions only.<sup>36</sup>

L-Leucine is an isomer of L-isoleucine and contains two chiral atoms,  $C^\alpha$  and  $C^\beta$ , with the difference between these two structures being the position of a methyl group. L-Leucine also crystallizes in the monoclinic  $P2_1$  space group, with two bimolecular asymmetric units in the unit cell. Figure 1b shows the molecular structures of L-leucine packed in their crystal lattice, showing the similarity of their molecular packing to L-isoleucine. The cell parameters of the lattice are  $a = 9.5620$ ,

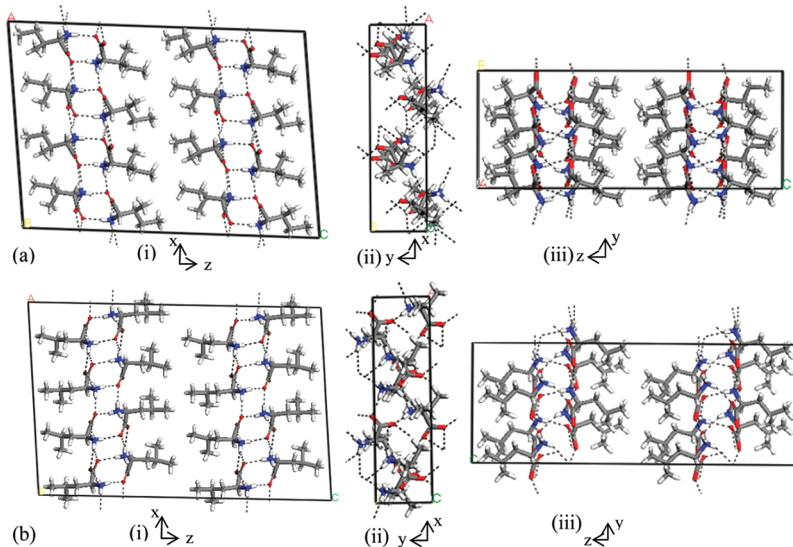


**Figure 1.** Molecular structure of (a) L-isoleucine crystal lattice and (b) L-leucine crystal lattice; in the order of: (i) view of crystal lattice showing the hydrogen bond network from the *y*-direction; (ii) view from the *z*-direction; and (iii) view from the *x*-direction.

$b = 5.3010$ ,  $c = 14.5190 \text{ \AA}$ , and  $\beta = 94.200^\circ$ . This similarity in crystal packing would suggest that L-leucine might be an interesting additive to study in L-isoleucine crystallization.

**Computational Methods.** The modeling of crystal growth morphology was carried out using two computational program packages, i.e. Habit98, a developmental version of Habit95,<sup>33</sup> and Material Studio (MS), from ACCELRYS, in which the calculation involves the determination of atomic charges, proton transfer energy, and lattice energy.

**Atomic Charges and Proton Transfer Determination.** The atomic charges were calculated by using two methods: the AM1 method in MOPAC<sup>37</sup> and density functional theory (DFT) of the quantum mechanical code in Material Studio. AM1 is a semiempirical method that can be adopted to calculate the molecular conformation and electronic properties, while the DFT quantum code in MS is an ab initio method, which is believed to be more accurate in estimating the electronic properties of atoms.<sup>37</sup> The AM1 calculation in MOPAC was performed using a single self-consistent-field method (keyword 1SCF), meanwhile the other three charges types, i.e. the electrostatic potential fitting (ESP), Mulliken,<sup>38</sup> and Hirshfeld,<sup>39</sup> were calculated in Material Studio by using the DFT quantum mechanical code with a BLYP gradient-corrected functional correlation, an “all electrons” core treatment, and the DNP basis set. Meanwhile, the proton transfer energy (used to calculate an experimental lattice in eq 3) was also determined by using the DFT quantum code, adopting the same setting as the atomic charges determination above. The difference of the minimized energies between both neutral and zwitterion structure was taken as the proton transfer energy.

**Lattice Energy Determination and Morphology Prediction.** Both the Habit98 and Material Studio programs were used to calculate the lattice energy and simulate the L-isoleucine morphology using the attachment energy summation method. They involve a measure of energy release due to the relative growth rate and addition of the growth slice to a growing crystal.<sup>40,41</sup> The Habit98 program calculates and identifies the important interatomic and intermolecular bonds in the lattice structure. It records the interaction between one origin molecule of the asymmetric unit and the second

molecule and asymmetric unit. The directions U, V, and W are multiples of the unit cell dimensions within the asymmetric units in a unit cell (*Z*) and molecules in the asymmetric unit (*J*). The suitability of the potential functions used in the lattice energy calculation was also assessed on the basis of the accuracy of the calculated lattice energy. The modeling procedures adopted by Habit98 were as follows: The L-isoleucine structure was obtained from CSD. By using the AM1 calculation method in MOPAC, the structure was subjected to geometry optimization in two stages, whereby first just the hydrogen atoms were relaxed and second all the atoms were relaxed. The output from this process also yields the atomic charges. The Momany<sup>42</sup> potential function together with atomic charges and the refined molecular geometries in MOPAC were used to calculate the interatomic optimization and attachment energy. The crystal morphology was plotted using Shape software.<sup>43</sup>

In Material Studio, the potential functions used were Compass,<sup>44</sup> CVFF,<sup>45</sup> and Universal. Compass is a potential function for which most of the parameters were derived from ab initio calculation while the rest of the parameters were fitted empirically. CVFF is a generalized valence potential function whose parameters are fitted to small organic crystals and gas phase structures such as amides, carboxylic acids, and handle peptides, proteins, and a wide range of organic systems. Meanwhile, the Universal potential function is known to be moderately accurate for predicting the geometries and conformational energies of organic molecules, some inorganics, and metal complexes. The morphology prediction of L-isoleucine through the calculation of lattice energy using the MS program package was as follows: The L-isoleucine structure was obtained from CSD. The atomic charges determined by using the methods described earlier were assigned to the molecules. The structure was subjected to geometry optimization and then energy minimization by using the potential function mentioned earlier. In this work, geometry optimization refers to the process whereby the conformations of the molecules were kept fixed while allowing the packing forces to change. Meanwhile, the energy minimization process allows the whole structure to move and varies the packing force as well as the conformation of the structure.

The same set of the potential function also was used for the lattice energy calculation. The Ewald summation method<sup>46</sup> was used to calculate the nonbonded interactions including the van der Waals and electrostatic contributions. The resultant structure building the morphology from the modeling was cross-checked with the published structure to ensure the validity of the modeling approaches adopted. The selected potential function then was used for the assessment of additive incorporation on the crystal morphology surface.

**Calculation of Additive Binding.** The likelihood of additive incorporation on a surface ( $hkl$ ) of an L-isoleucine crystal was assessed through the determination of “differential” slice energy, as defined by Poornachary et al.<sup>6</sup> as being the difference between the slice energy of pure L-isoleucine of the cleaved ( $hkl$ ) surface (termed as the reference energy,  $E_{\text{ref}}^{\text{slice}}$ ) and that,  $E_{\text{add}}^{\text{slice}}$ , of an impurity incorporated in the ( $hkl$ ) layer. This slice energy is not the same as that defined in eq 1, as this energy is calculated as incorporation of one additive molecule (by replacing the host molecule with the additive molecule) into the  $hkl$  slice of the host molecule. In this work, we would prefer to adopt this slice energy as a metaphor on the ability of the additive molecule to incorporate in the morphology surface. The additive molecule was optimized by minimizing the energy of the molecule. The L-leucine molecule was then docked on the selected surface of L-isoleucine, replacing one molecule of host L-isoleucine. The position of the additive molecule was adjusted such that its amino group superimposed the amino group of the host molecule that was being replaced. The substitution of a L-isoleucine molecule by both of the L-leucine conformers (A and B) was carried out in this study. The geometry and position of the docked molecule were optimized on the rigid  $hkl$  surface. The orientation of the L-leucine molecule with the lowest minimized energy was taken as the most stable configuration. The whole  $hkl$  surface containing a docked additive molecule then was relaxed and minimized again, with the associated energy ( $E_{\text{minimized}}$ ) being computed. The Compass potential function was used in an energy minimization calculation with the Ewald summation method for nonbonded interactions. The energies of the optimized geometries of both the surface and the docked molecule were also calculated, and they were denoted by  $E_{\text{surface}}$  and  $E_{\text{additive}}$ , respectively. The slice energy,  $E_{\text{add}}^{\text{slice}}$ , of an additive molecule on the facet site was calculated by using eq 4:

$$E''_{\text{slice}} = E_{\text{minimized}} - E_{\text{surface}} - E_{\text{inhibitor}} \quad (4)$$

The adsorption of additive molecule was considered as possible when the slice energy generated by the additive molecule substituted on the host surface,  $E''_{\text{slice}}$ , is more negative than the energy of the reference system,  $E'_{\text{slice}}$ . The graphic of additive substitution in the crystal surface slice is shown in Figure 5.

## RESULTS AND DISCUSSION

### Atomic Charges, Proton Transfer, and Lattice Energy Calculation.

In calculating the lattice energy, four types of charge sets were used in this work: AM1, Hirshfeld, Mulliken, and electrostatic potential (ESP). The result of the charge set shows that the atomic charges generated (supplied as Supporting Information) are very dependent on the charge sets used. The same observation was also noted by Poornachary et al.<sup>6</sup> in their work in determining the lattice energy of glycine.

**Table 1. Lattice Energies (kcal/mol) of L-Isoleucine Computed Using Different Potential Function and Charge Types**

potential function	charge type	$E_{\text{latt}}$ (kcal/mol)	percentage error (%)
Momany	experimental	-66.01	
	AM1	-65.20	1.24
	Mulliken	-64.04	3.08
	Hirshfeld	-55.64	18.64
Compass	ESP	-66.21	0.30
	AM1	-89.553	26.29
	Mulliken	-81.26	18.77
	Hirshfeld	-63.36	4.18
Universal	ESP	-101.31	34.84
	AM1	-81.15	18.66
	Mulliken	-72.99	9.56
	Hirshfeld	-59.27	11.36
CVFF	ESP	-82.95	20.42
	AM1	-91.94	28.20
	Mulliken	-84.89	22.24
	Hirshfeld	-68.21	3.219
	ESP	-102.14	35.37

Table 1 shows the calculated lattice energy corresponds to potential functions and assigned charge sets. The lattice energy calculated using Habit98 is -30.77 kcal/mol, but in the Momany potential function and the atom–atom summation method used in Habit98, the proton transfer energy was not taken into account.<sup>29,47</sup> The Momany potential function was first developed for neutral amino acids, and then its application was extended to zwitterion amino acids, and due to this, the proton transfer contribution was not considered. The proton transfer energies for some amino acids are in the range between 21.32 and 34.32 kcal/mol,<sup>30,31</sup> but to our knowledge no value for L-isoleucine has ever been recorded. For discussion purposes, the lattice energy calculated by using Momany as the potential function and the AM1 charge type is used as an example. The calculated proton transfer energy for L-isoleucine (i.e., -34.43 kcal/mol) was added to -30.77 kcal/mol (simulated lattice energy), which then gives the total lattice energy calculated by using the atom–atom method to be -65.20 kcal/mol. Comparison with the experimental lattice energy (using eq 3) gives a small percentage error of 1.24%, which indicates that the Momany potential function used together with the AM1 charge set is suitable for morphology prediction of L-isoleucine. The experimental heat of sublimation used in eq 3 was -29.87 kcal/mol.<sup>48</sup>

The lattice energies computed in Table 1 show that the calculated values are sensitive to the charge sets and potential functions used, in which the values vary between -55.64 and -102.14 kcal/mol. Meanwhile, comparison between the experimental and predicted lattice energies determined using the MS program shows that the percentage deviation varies between 0.30 and 35.37%. The lattice energy calculated by using the Compass potential function, adopting atomic charges determined using the Hirshfeld method, shows a good fit to the experimental lattice energy with a percentage error of 4.18%. The CVFF potential function used together with the Hirshfeld charge set also shows good agreement between predicted and experimental lattice energies. Nevertheless, both the ESP and AM1 charge sets used with any types of potential functions (but with the exception with Momany potential function) show a large deviation from the experimental value. In this work, we would like to consider the lattice energy calculated using the

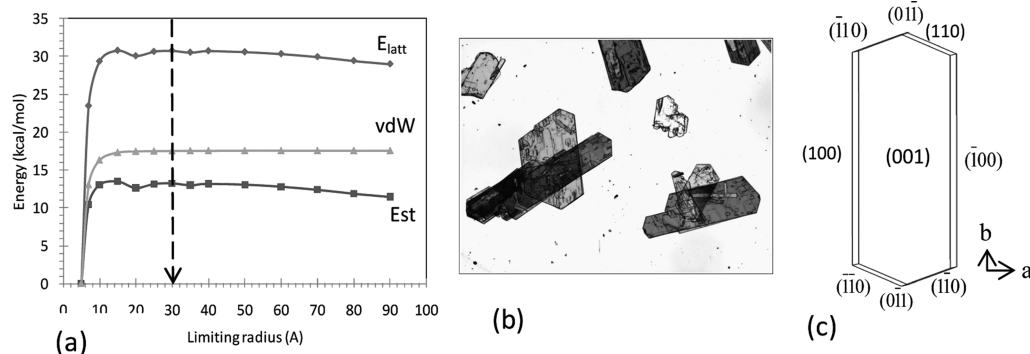


**Figure 2.** (a) Simulation of crystal lattice energy as a function of the interaction distance, showing the lattice energy ( $E_{\text{latt}}$ ) as a summation from electrostatic ( $E_{\text{st}}$ ) and van der Waals energies ( $\text{vdW}$ ), determined using Habit98. The optimum distance for the intermolecular interactions from the central molecule was taken at an ca. 30 Å radius, where the energy leveled off with the distance of atoms to the central atom. (b) L-Isoleucine crystal grown in water and (c) simulated crystal morphology plotted using Shape Software based on the attachment energy from Habit98. The result shows good agreement between the two.

potential function and charge set with an error less than 5% as a good fit to the experimental lattice energy.

The analysis of the lattice energy using Habit98 for the summation of the intermolecular interactions as a function of the limiting radius from the central molecule is shown in Figure 2a. The summation of the nonbonded van der Waals and electrostatic charges is equal to the lattice energy. The convergence was reached via summation of the intermolecular interaction of the origin molecule with the neighboring molecule within a limit of a 30 Å radius. The result shows that the electrostatic charge contributes about 43% of the lattice energy, indicating the dipolar effect is significant to the formation of this crystal.

#### Morphological Prediction of L-Isoleucine Crystal.

Figure 2b shows the morphology of an L-isoleucine crystal grown in distilled water together with the predicted morphology (Figure 2c), revealing a good correlation to the predicted L-isoleucine. The morphology shows a leafy hexagonal shape, thin elongated with a corner angle of about 120° each. The morphology is bounded by dominant (001) and (00̄1) facets elongated along the *b*-axis, with the long and thin (100) and (10̄0) facets and the angled (110), (11̄0), (11̄0), and (110) facets at the top and bottom sides of the crystal. Facets (011) and (01̄1) are at the top and bottom of the morphology, but these facets are not clearly visible. The distribution of lattice energy (as a summation of slice and attachment energies) calculated using attachment energy and BFDH methods of visible facets of the morphology is shown in Table 2. The dominating (001) facet is with the lowest attachment energy of -0.07 kcal/mol and the slowest growing face while facet (011) and its symmetry facet of (01̄1) are with the highest attachment energies and the smallest growing faces. This phenomenon can be observed from the surface chemistry of the large face of (001) and its symmetrical surface of (00̄1) (Figure 3a, b), in which it is built by the hydrophobic region of the molecular structure, where only the weak van der Waals interaction dominates the crystal surface. Meanwhile, facets (110), (11̄0), and (011) and all their symmetries have large negative attachment energies, which result in fast growing but less morphologically important facets. The hydrogen bond interaction can be clearly observed from the surface chemistry of these facets (Figure 3e–j). It can be seen that there are oxygen atoms (which are known to have high polarity) on the terminating (110) and (011) facets and their respective

**Table 2. Face Multiplicity and *d*-Spacing from BFDH Analysis Showing the Respective Attachment and Slice Energy Calculated Using the Habit98 Program<sup>a</sup>**

face	multiplicity	<i>d</i> -spacing	attachment energy (kcal/mol)	slice energy (kcal/mol)
(001)	2	13.95	-0.07	-30.70
(100)	2	9.51	-4.18	-26.59
(01̄1)	2	4.66	-20.54	-10.24
(110)	2	4.39	-19.29	-11.49
(11̄0)	2	4.39	-19.29	-11.49

<sup>a</sup>The distribution of energies corresponds to the lattice energy calculated via the atom–atom method, i.e., -30.77 kcal/mol, and the proton transfer energy factor was not included.

symmetry surfaces which are believed to contribute to the high electrostatic energy for these faces. Interestingly enough, the surface chemistry of facets (110), (11̄0), and (011) shows different structural arrangements from their respective symmetric facets due to the nature of this polar L-isoleucine crystal (see Figure 3e–j), even though each symmetrical facet pair has the same attachment and slice energies. Nevertheless, both (001) and (100) facets (Figure 3a, c) do not show any significant difference in surface molecular arrangement with their respective symmetrical pairs of facets (00̄1) and (10̄0) (Figure 3b, d).

In this work, the most important intermolecular interactions were identified and presented in Table 3. The interactions recorded in Table 3 were between origin molecule J of the asymmetric unit Z at origin position [000] and the second molecule J and asymmetric unit Z, following the UVW direction. Analysis of the bonds carried out shows that the dominating interactions in the crystal lattice are between the carbonyl oxygen and the amino hydrogen, where the energies are twice as large as the next strongest bond.

The result shows that the energies decrease with interatomic distance. The van der Waals energy, which accounted for both attractive and repulsive energies, dominates the short distance molecular and atomic interaction (bond types a, b, c, e, and f), while the effect of the Coulombic energies is still apparent at longer distance interactions (bond types g and h). Charge separation in the L-isoleucine zwitterion molecules produces strong dipole and large atomic charges of the amino and

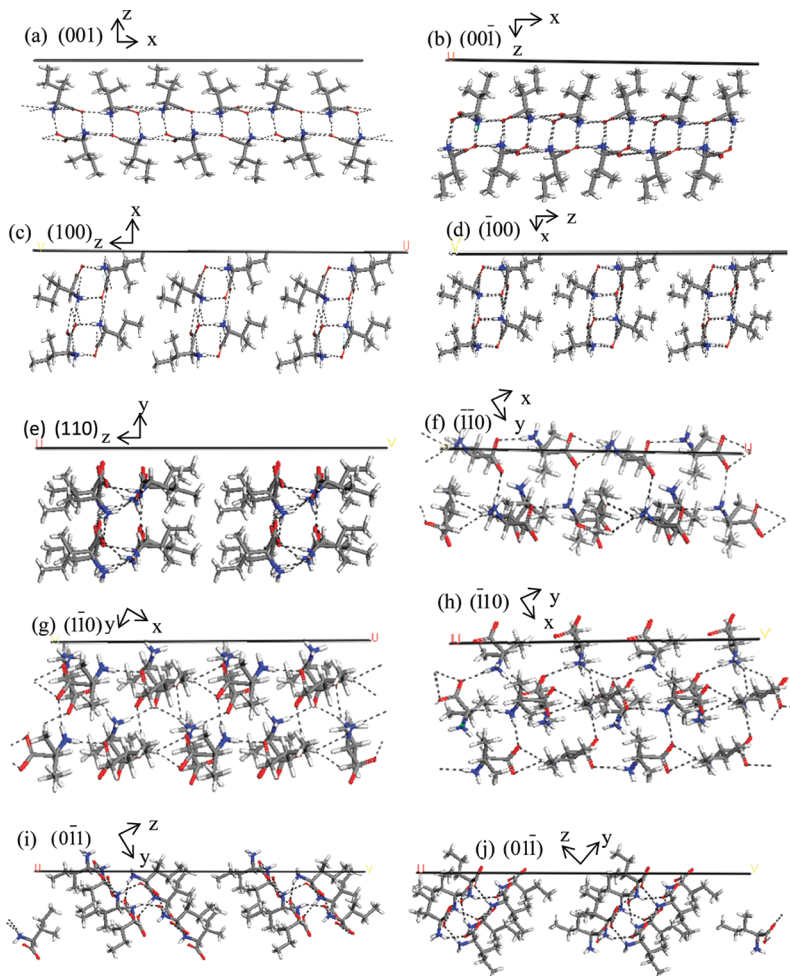


**Figure 3.** Molecular packing diagram of L-isoleucine illustrating the surface chemistry of crystal facets: (a) (001), (b) (00 $\bar{1}$ ), (c) (100), (d) ( $\bar{1}00$ ), (e) (110), (f) ( $\bar{1}\bar{1}0$ ), (g) ( $\bar{1}\bar{1}0$ ), (h) ( $\bar{1}10$ ), (i) (0 $\bar{1}1$ ), and (j) (01 $\bar{1}$ ), determined using the routine available in the MS program package; the force field used was Compass.

**Table 3. Most Important Intermolecular Bonds (Calculated Using Habit98) for L-Isoleucine Crystal (in kcal/mol) between the Origin Molecules of [000ZJ] and the Next Molecule of [UVWJ'Z']<sup>a</sup>**

bond type	ZJ[UVWJ'Z']	distance (Å)	energies (kcal/mol)		
			van der Waals	Coulomb	total
a	21[-10-1]12	5.82	-2.25	-4.14	-6.39
b	11[-100]12	5.58	-1.59	-4.53	-6.12
c	11[0-10]12	5.47	-1.83	-4.24	-6.07
d	12[111]21	7.79	-0.48	-2.58	-3.06
e	11[0-10]11	5.30	-2.25	-0.45	-2.70
f	12[0-10]12	5.30	-2.15	-0.42	-2.57
g	11[101]22	7.95	-0.19	-1.35	-1.55
h	12[020]11	9.21	-0.08	-1.02	-1.11
			total	-29.57	

<sup>a</sup>J is the molecule number in the asymmetric unit, and Z is the number of asymmetric units in a unit cell. The proton transfer energy factor was not included.

carboxyl groups, which makes the Coulombic interactions potentially the strongest physical interactions in this work.

**Additive Calculation on L-Isoleucine Morphology Facets.** Figure 4 shows the morphology of L-isoleucine with

the presence of additive L-leucine. The labels of facets on the morphology of L-isoleucine (Figure 4) are only an illustration,

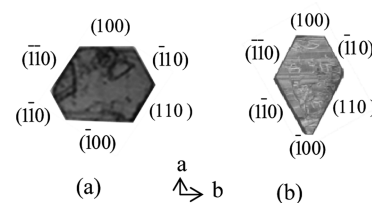


**Figure 4.** (a) Habit modifications due to L-leucine (10 wt %, w/w L-isoleucine). (b) Morphology of L-isoleucine with additive L-leucine (37 wt %, w/w L-isoleucine).

as the exact position of the facets was not determined. As mentioned earlier, L-isoleucine is a polar crystal which makes faces ( $hkl$ ) not necessarily symmetrical representations of faces ( $\bar{h}\bar{k}\bar{l}$ ), which in turn affects the result of attachment of additive on the surface. The addition of 10 wt % (w/w) L-leucine to L-isoleucine solution results in a change of morphology in which a more isometric hexagonal shape crystal was recovered with growth reduction along the  $b$ -axis of the L-isoleucine crystal, and increasing the amount of L-leucine added results in shorter morphology along the  $b$ -axis. The growth rate of the (100)

facet became faster, and at this point, each side has almost the same dimensions, which suggests that their growth rates are almost the same. Further addition of L-leucine (37% w/w) widens the crystal along the *a*-axis, and the (100) face becomes the smallest surface of the crystal and at the same time increases the area of the (110), ( $\bar{1}10$ ), ( $\bar{1}\bar{1}0$ ), and (1 $\bar{1}0$ ) facets, which become more morphologically important surfaces. In all cases, the (001) and its symmetry facet remain the most dominant. The effect of additives on the (011) and (0 $\bar{1}1$ ) faces could not be readily observed here, as these facets were found to be very small. Similar observations also were noted by Koolman and Rousseau<sup>20</sup> on their work with L-leucine as an additive to L-isoleucine solution; albeit, in this work, the growth rate and the surface area of each face were not measured.

Table 4 shows the change in energy due to incorporation of L-leucine molecule in each possible crystallographic site, along

that the incorporation of additives onto these facets would not be favored. Interestingly, both the (100) and (001) facets, which were identified, have the same surface molecular arrangement, as their respective symmetries (Figure 3a–d) show the same impurity incorporation behavior between their symmetries. However, all the other facets (with the exception of facets (1 $\bar{1}0$ ) and ( $\bar{1}\bar{1}0$ )) and their supposedly symmetrical surfaces show contrast impurity incorporation behavior between their respective symmetries. This behavior is expected, as they have different surface molecular arrangements due to the polar nature of the L-isoleucine molecule. The molecule substitution slice energies presented in Table 4 are for the substitution of molecule B onto the surfaces. Nevertheless, the substitutions of molecule A of L-leucine onto L-isoleucine surfaces were also carried out, and the result shows the same impurity inclusion behavior as shown by Table 4, but with different numerical values of slice energies. However, there is also some exception to this behavior in which facet (0 $\bar{1}1$ ) favors the inclusion of molecule A into its surface, as opposed to the result given in Table 4 for inclusion of molecule B. Meanwhile, facet (011) does not favor inclusion of molecule A into its surface, in contrast to molecule B inclusion.

Inspection of atomic interaction based on the visible hydrogen bonds network for facets (001) and (100) in Figure 5a,b shows that substituting L-leucine molecules affects the hydrogen bond network, which includes both the van der Waals and columbic interactions. In the MS simulations, the maximum distance for the H-bond to be visibly available was set to be 2.5 Å. For facet (001), the tilted oxygen of the carbonyl group orientation (marked as A in Figure 5a) results in a longer atomic distance (more than 2.5 Å) to the neighboring hydrogen amino group. This in turn caused a reduction of the strong  $\text{COO}^- \cdots \text{H}_3\text{N}$  interaction of the system and, hence, lowered the bonding energy. The interatomic distances between the carbon atom of L-leucine to neighboring carbon atoms of the host molecule on the (001) surface were measured, revealing the shortest distance to be about 2.1 Å, when compared to the shortest distance between carbon–carbon atoms of the original (001) L-isoleucine surface molecules, within the range of more than 3.7 Å. This result is consistent with the finding by Kitaigorodsky,<sup>49</sup> whom concluded that, under normal conditions, the minimum distance between nonbonded carbon atoms is 3.0 Å and 2.9 Å.

**Table 4. Slice Energies Calculated for the Additive L-Leucine (Molecule B) on the Growth Faces of L-Isoleucine<sup>a</sup>**

growth face	minimized energy, $E_{\text{minimized}}$	surface energy, $E_{\text{surface}}$	additive inhibition energy, $E_{\text{inhibitor}}$	slice energy with additive, $E''_{\text{slice}}$	slice energy for the reference system, $E'_{\text{slice}}$
(001)	-12503.9	-12356.3	-43.6	-104.0	-112.2
(00 $\bar{1}$ )	-9325.3	-9168.9	-44.1	-279.7	-317.7
(100)	-22040.6	-21858.5	-42.4	-139.7	-98.2
( $\bar{1}00$ )	-40144.9	-39813.8	-39.9	-211.1	-194.8
(110)	-21150.8	-20996.1	-41.3	-113.4	-105.1
( $\bar{1}\bar{1}0$ )	-17028.0	-16885.0	-40.9	-102.1	-104.03
( $\bar{1}0$ )	-16848.8	-16714.1	-41.8	-92.8	-808.4
( $\bar{1}\bar{1}0$ )	-16979.9	-16848.0	-33.0	-98.8	-591.7
(011)	-17028.6	-15557.6	-13.1	-1457.9	-170.97
(0 $\bar{1}1$ )	-16831.0	-16693.3	-46.4	-91.3	-138.4

<sup>a</sup>The potential function used was Compass, and the energies have the unit of kcal/mol.

with the host and additive slice energies. The results show that facets (100), ( $\bar{1}00$ ), (110), and (011) are the most likely binding sites for the L-leucine additive to incorporate, since  $E_{\text{slice}}''$  is more negative than the  $E_{\text{slice}}'$  of the pure L-isoleucine slice (the reference system). The slice energies determined for facets (011), (001), ( $\bar{1}10$ ), (1 $\bar{1}0$ ), ( $\bar{1}0$ ), and (0 $\bar{1}1$ ) indicate

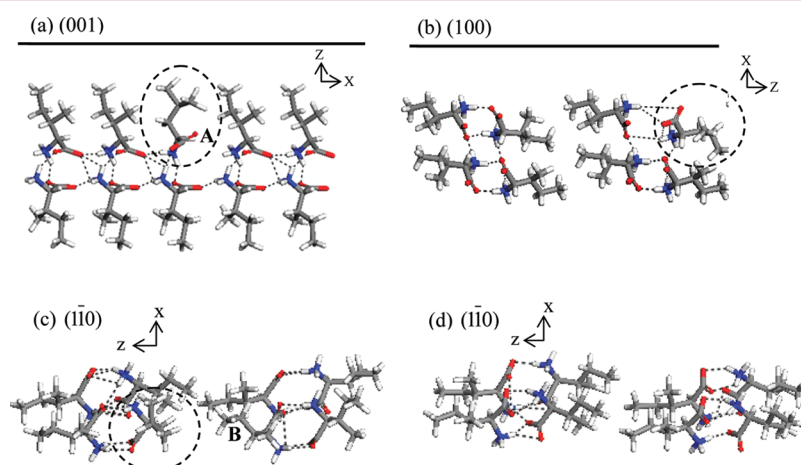


**Figure 5.** Substitution of the additive L-leucine on (a) (001) surface; (b) (100) surface; and (c) (110) surface. (d) The orientation of L-isoleucine molecules on the surface plane (110), without the presence of additive. The additives were shown by the dotted circles.

for extreme conditions. The proximity of nonbonded carbon atoms with distance lesser than the minimum distance between neighboring molecules due to the presence of an additive molecule results in overlapping of the electron shell and, hence, gives rise to a strong repulsion between the carbon atoms,<sup>20</sup> providing a rationalization for the prediction that incorporation of an L-isoleucine molecule at this site was not favored. Examination of the incorporation of L-leucine molecules at the slice surface of (100) (Figure 5b) reveals that the additive fitted nicely into the surface of the slice. The tilted carboxyl group of L-leucine (in circle) reduces the distance between the carboxyl and amino groups, and this phenomenon probably creates stronger hydrogen bonds, which makes the additive inclusion favorable to this site. Comparison between the substituted L-leucine molecule and the original arrangement of the L-isoleucine molecule on the (1 $\overline{1}$ 0) slice surface is shown in Figure 5c and d, respectively. From this, it is evident that the presence of L-leucine in the host surface (shown by a circle in Figure 5c) resulted in repositioning of the host molecule (marked as B) of the surface, causing disruption to the interatomic interactions (and hence the total bonding energy). Such an unfavorable incorporation to this site perhaps explains the less negative energy for the slice energy,  $E_{\text{slice}}$ , value with the presence of additive substituted on the surface of the facet (see Table 4).

The assessment of the effect of L-leucine as an impurity to L-isoleucine crystals also was carried out by Koolman and Rousseau.<sup>20</sup> They concluded that the steric hindrance associated with substituting an L-leucine molecule into an L-isoleucine lattice brought carbon atoms in adjacent layers into very close proximity along the *b*-axis. This in turn caused repulsion of an oncoming crystal layer and a reduction of growth in the *b*-axis direction. From their work, analysis of crystals recovered from a solution containing 0.13 mol of L-leucine/mol of L-isoleucine by using HPLC revealed that, on average, the crystals contain one molecule of L-leucine in every eight molecules of L-isoleucine. Work by Givand et al.<sup>9</sup> concluded that the incorporation of L-leucine as an impurity into the L-isoleucine crystal is by lattice substitution and is controlled by the thermodynamics of the solution system, i.e. through their relatively pure component solubilities in the same solvent. Their experiments, involving L-leucine, L-valine, and L-isoleucine with solubilities of 25 g/L, 87 g/L, and 40 g/L in water at 20 °C, were consistent with the hypothesis that compounds with lower solubilities would be expected to have a higher tendency to be contaminated by host molecules with higher solubility, compared to the converse case. Hence, a relationship linking the amino acid impurity distribution coefficients and the amino acid solubility ratio was established.

## CONCLUSIONS

From this work, we have explored methods to predict the shape of the L-isoleucine crystal grown from distilled water. The computational methods used give good agreement with the observed crystal morphology, which is characterized by an elongated hexagonal shape associated with ten crystal faces: (001), (00 $\bar{1}$ ), (100), ( $\bar{1}$ 00), (110), (1 $\bar{1}$ 0), (01 $\bar{1}$ ), (0 $\bar{1}$ 1), (110), and (1 $\bar{1}$ 0). Comparison between simulated and experimental lattice energies for some of the potential functions shows a percentage error of less than 5% between them. This result suggests that selection of the potential function together with charge sets could provide suitable intermolecular parameters for the prediction of the morphology of L-isoleucine crystals. The atom-specific energy contribution to the lattice energy was

found to be dominated by interactions between the carbonyl group oxygens and the amino group hydrogens, which is consistent with the large electrostatic contribution to the lattice energy. Assessment of the atomic interactions and modified slice energies associated with potential additive binding reveals L-leucine additive molecules preferentially could adsorb on the (100), (1 $\overline{1}$ 0), (01 $\overline{1}$ ), and the (110) crystal surfaces, hence altering the L-isoleucine crystal morphology and forming a more isometric hexagonal shape crystal.

## ASSOCIATED CONTENT

### S Supporting Information

Tables of calculated atomic charges of L-isoleucine, and figure showing the structure of L-isoleucine. This material is available free of charge via the Internet at <http://pubs.acs.org>.

## AUTHOR INFORMATION

### Corresponding Author

\*Telephone: +60 3 5543 6315. Fax: +60 3 5543 6300. E-mail: nornizar@salam.uitm.edu.my.

### Notes

The authors declare no competing financial interest.

## ACKNOWLEDGMENTS

The authors would like to express their gratitude to the Ministry of Science and Technology, Malaysia, for funding of this work, which was carried out in collaboration with the Institutes of Particle Science and Engineering and Process R&D, at the University of Leeds, in the U.K. One of us (N.A.) would like to thank Universiti Teknologi MARA for the sponsorship of this Ph.D. study. This work is part of Grant 02-02-02-0001 PR0023/11-06 and Grant FRGS 212001100002.

## REFERENCES

- (1) Matsuoka, M.; Yamanobe, M.; Tezuka, N.; Takiyama, H.; Ishii, H. *J. Cryst. Growth* **1999**, *198/199*, 1299–1306.
- (2) Dressler, D. H.; Hod, I.; Mastai, Y. *J. Cryst. Growth* **2008**, *310*, 1718–1724.
- (3) Hammond, R. B.; Pencheva, K.; Roberts, K. J. *J. Phys. Chem. B* **2005**, *109*, 19550–19552.
- (4) Lin, C. H.; Gabas, N.; Canselier, J. P.; Pepe, G. *J. Cryst. Growth* **1998**, *191*, 791–802.
- (5) Dhanaraj, G.; Shripathi, T.; Bhat, H. L. *J. Cryst. Growth* **1991**, *113*, 456–464.
- (6) Poornachary, S. K.; Chow, P. S.; Tan, R. B. H. *J. Cryst. Growth* **2008**, *310*, 3034–3041.
- (7) Towler, C. S.; Davey, R. J.; Lancaster, R. W.; Price, C. J. *J. Am. Chem. Soc.* **2004**, *126*, 13347–13353.
- (8) Weissbuch, I.; Lahav, M.; Leiserowitz, L. *Cryst. Growth Des.* **2003**, *3*, 125–150.
- (9) Givand, J. C.; Chang, B.-K.; Teja, A. S.; Rousseau, R. W. *Ind. Eng. Chem. Res.* **2002**, *41*, 1873–1876.
- (10) Dalhus, B.; Görbitz, C. H. *Acta Crystallogr.* **2000**, *B56*, 720–727.
- (11) Zumstein, R. C.; Rousseau, R. W. *Ind. Eng. Chem. Res.* **1989**, *28*, 1226–1231.
- (12) Brown, M. G.; Rousseau, R. W. *Biotechnol. Prog.* **1994**, *10*, 253–257.
- (13) Gude, M. T.; Meuwissen, H. H. J.; van der Wielen, L. A. M.; Luyben, K. *Ind. Eng. Chem. Res.* **1996**, *35*, 4700–4712.
- (14) Anuar, N.; Wan Daud, W. R.; Roberts, K. J.; Kamarudin, S. K.; Tasirin, S. M. *Cryst. Growth Des.* **2009**, *9*, 2853–2862.
- (15) Day, G. M.; Cooper, T. G. *CrystEngComm* **2010**, *12*, 2443–2453.
- (16) Givand, J. C.; Rousseau, R. W.; Ludovice, P. J. *J. Cryst. Growth* **1998**, *194*, 228–238.

- (17) Almeida, F. M.; Freira, P. T. C.; Lima, R. J. C.; Reme' dios, C. M. R.; Mendes Filho, J.; Melo, F. E. A. *J. Raman Spectrosc.* **2006**, *37*, 1296–1301.
- (18) Givand, J. C.; Teja, A. S.; Rousseau, R. W. *AICHE J.* **2001**, *47*, 2705–2712.
- (19) Furuta, S.; Rousseau, R. W.; Teja, A. S. *J. Cryst. Growth* **1995**, *148*, 197–200.
- (20) Koolman, H. C.; Rousseau, R. W. *AICHE J.* **1996**, *42*, 147–153.
- (21) Görbitz, C. H. *THEOCHEM* **2006**, 9–17.
- (22) Hartman, P.; Perdock, W. G. *Acta Crystallogr.* **1955**, *8*, 521–524.
- (23) Hartman, P.; Bennema, J. *J. Cryst. Growth* **1980**, *49*, 145–156.
- (24) Clydesdale, G.; Roberts, K. J. In *Science and Technology of Crystal Growth*; Kluwer Academic Publishers: The Netherlands, 1995; pp 179–192.
- (25) Clydesdale, G.; Roberts, K. J.; Walker, E. M. In *Molecular Solid State: Syntheses, Structure, Reactions, Applications: Theoretical Aspects and Computer Modelling*; Gavezzotti, A., Eds.; John Wiley and Sons: New York, 1996; Vol. 2, Chapter 7, pp 203–232.
- (26) Clydesdale, G.; Roberts, K. J.; Docherty, R. In *Controlled Particle, Droplet and Bubble Formation*; Wedlock, D. J., Eds.; Butterworths-Heinemann: London, 1994; Chapter 4, pp 119–121.
- (27) Hammond, R. B.; Pencheva, K.; Roberts, K. *J. Cryst. Growth Des.* **2006**, *6*, 1324–1334.
- (28) Clydesdale, G.; Roberts, K. J.; Telfer, G. B.; Saunders, V. R.; Pugh, D.; Jackson, R. A.; Meenan, P. *J. Phys. Chem. B* **1998**, *102*, 7044–7049.
- (29) Pencheva, K. Ph.D. Thesis, University of Leeds: United Kingdom, 2006.
- (30) No, K. T.; Cho, K. H.; Kwon, O. Y.; Jhon, M. S.; Scheraga, H. A. *J. Phys. Chem.* **1994**, *98*, 10742–10752.
- (31) Voogd, J.; Derissen, J. L.; van Duijneveldt, F. B. *J. Am. Chem. Soc.* **1981**, *103*, 7701–7706.
- (32) Cooper, T. G.; Hejczyk, K. E.; Jones, W.; Day, G. M. *J. Chem. Theory Comput.* **2008**, *4*, 1795–1805.
- (33) Day, G. M. *Crystallogr. Rev.* **2011**, *17*, 3–52.
- (34) Torii, K.; Iitaka, Y. *Acta Crystallogr.* **1971**, *B27*, 2237–2246.
- (35) Aitipamula, S.; Desiraju, G. R.; Jaskolski, M.; Nangia, A.; Thaimattam, R. *CrystEngComm* **2003**, *5*, 447–450.
- (36) Görbitz, C. H.; Dalhus, B. *Acta Crystallogr.* **1999**, *B55*, 424–431.
- (37) Steward, J. J. P. *J. Comput.-Aided Mol. Des.* **1990**, *4*, 1–45.
- (38) Mulliken, R. S. *J. J. Chem. Phys.* **1955**, *23*, 1833–1840.
- (39) Hirshfeld, F. L. *Theor. Chim. Acta B* **1977**, *44*, 129–138.
- (40) Berkovitch-Yellin, Z. *J. Am. Chem. Soc.* **1985**, *107*, 8239–8253.
- (41) Docherty, R.; Clydesdale, G.; Roberts, K. J.; Bennema, P. *J. Phys. D: Appl. Phys.* **1991**, *24*, 89–99.
- (42) Momany, F. A.; Carruthers, L. M.; McGuire, R. F.; Scheraga, H. A. *J. Phys. Chem.* **1974**, *78*, 1595–1620.
- (43) Dowty, E. *Am. Mineral.* **1980**, *65*, 465–471.
- (44) Sun, H. *J. Phys. Chem. B* **1998**, *102*, 7338–7364.
- (45) Dauber-Osguthorpe, P.; Roberts, V. A.; Osguthorpe, D. J.; Wolff, J.; Genest, M.; Hagler, A. T. *Proteins: Struct., Funct., Genet.* **1988**, *4*, 31–47.
- (46) Ewald, P. P. *Ann. Phys.* **1921**, *64*, 253–287.
- (47) Bisker-Lieb, V.; Doherty, M. F. *Cryst. Growth Des.* **2003**, *3*, 221–237.
- (48) Chickos, J. S.; Acree, W. E. Jr. *J. Phys. Chem. Ref. Data* **2002**, *31*, 537–698.
- (49) Kitaigorodsky, A. I. *Molecular Crystals and Molecules*; Academic Press: New York, 1973.